Collision Frequencies between Fractal Aggregates and Small Particles in a Turbulently Sheared Fluid

XIAOYAN LI† AND BRUCE E. LOGAN*

Department of Chemical and Environmental Engineering, University of Arizona, Tucson, Arizona 85721

Three groups of aggregates with fractal dimensions of 1.89 ± 0.06, 2.21 ± 0.06, and 2.47 ± 0.10 were generated by coagulation of latex microspheres (2.85 μm) in a Jar-test (paddle-mixing) device. The collision rates between these fractal aggregates (200−1000 μm) and small (1.48 μm) particles were measured in the turbulent shear environment of the paddle mixer at mean shear rates of 2.1, 7.3, and 14.7 s^{-1}. Collision frequencies were 5 orders of magnitude higher than predicted by a curvilinear model but 2 orders of magnitude lower than predicted by a rectilinear model. Collision frequencies much higher than predicted by the curvilinear collision kernel were attributed to significant flow through the interior of the fractal aggregates. The fluid shear rate (G) and the aggregate fractal dimension (D) affected the collision frequency function (β) between fractal aggregates and small particles, resulting in $\beta \sim G^{1-0.33D}$. According to this relationship, as $D \rightarrow 0$, the aggregates become infinitely porous and β becomes proportional to G^1 as described by a rectilinear collision model based on aggregates sweeping out all fluid within their pathway. As aggregates become less fractal and $D \rightarrow 3$, β becomes relatively insensitive to the magnitude of G as predicted by a curvilinear model.

Introduction

The capture of suspended small particles by large porous aggregates is of interest in the description of particle transport in the turbulent environment of natural waters as well as water and wastewater treatment systems. The kinetics of particle coagulation by shear motion was originally formulated based on a rectilinear model in which collision frequencies are proportional to the mean shear rate (*1*, *2*). The rectilinear model is known to overpredict particle collisions since this model does not account for hydrodynamic interactions and short-range forces between particles (*3*, *4*). These limitations have led to the development of various curvilinear models that predict that increases in the shear rate do not significantly enhance the coagulation rate (*3*, *5*). Since curvilinear models were established for solid particles and do not include a mechanism for the flow through permeable aggregates, they may underestimate the collision frequency function for highly porous aggregates (*6*−*8*).

Aggregates produced by coagulation are fractal (*9*−*11*), and therefore, they have a non-uniform mass distribution, a structure resulting from the coagulation of small and more densely packed clusters into larger and overall less dense aggregates (*12*, *13*). Large pores formed between these clusters within the aggregates permit streamlines to cross the aggregate surface. In a previous study, the aggregate permeabilities derived from observed settling velocities were found to be 3 orders of magnitude greater than predicted by a permeability model assuming a uniform distribution of primary particles throughout the aggregate (*13*). As a result of significant flow through the interior of the aggregates, the collision frequencies between the settling fractal aggregates and suspended small particles were much higher than predicted using a curvilinear collision model.

In the present study, we measured the collision frequencies between fractal aggregates and microspheres under turbulent shear conditions. The effect of the mean shear rate on collision frequencies between the fractal aggregates and small particles was experimentally tested by measuring the capture rates of microspheres by the aggregates suspended in solutions stirred at different mean shear rates. The importance of the fractal dimension of the aggregates on their collision frequency function was examined by correlating the collision frequency function with the aggregate size and mean fluid shear rate.

Methods

Experimental Section. *Generation of Fractal Aggregates.* The aggregates used in shear coagulation experiments were generated from red-colored latex microspheres 2.85 μm in diameter with a density of 1.05 g cm^{-3} (Polysciences) in a Jar-test device with flat paddles (7.6 × 2.5 cm^2) (Model 7790-400, Phipps and Bird). Three groups (A, B, and C) of aggregates were generated under different coagulation conditions. Group A and group B aggregates were formed by fast and slow coagulation, respectively, as previously described (13). Group C aggregates were formed through breakup and re-coagulation of Group B aggregates by rapidly stirring an aggregated suspension twice (2 min each time, $G = 49-62$ s^{-1}) over a 2-h period and then re-coagulating the suspension at a lower shear rate ($G = 6.2$ s^{-1}). Aggregates in group C were expected to be denser and have a higher fractal dimension than aggregates in groups A and B since they were formed by restructuring previously coagulated aggregates (*14*, *15*).

Coagulation Experiments. Coagulation experiments between aggregates and small particles were performed in 1000-mL beakers in the Jar-test device. Each beaker was filled with 500 mL of a 2% NaCl suspension of fluorescent yellow-green (YG) latex microspheres 1.48 μm in diameter (Polysciences). This high ionic strength solution was used to destabilize the particles. The solution pH was kept at ~8.5, and the YG bead concentrations varied from 10^5 to 5×10^5 mL^{-1} in order to adjust coagulation rates between aggregates and beads.

For each of three aggregate groups (A, B, and C), coagulation experiments between aggregates and small particles were conducted at three different paddle rotation speeds (6, 15, and 25 rpm), resulting in nine data sets. During each experiment, coagulation rates were measured at times of $T = 5$, 10, 20, and 40 min. In each coagulation experiment, several red-bead aggregates were introduced into a YG bead suspension using a rubber dropper bulb with a 1-mL pipet tip cut midway between its ends to provide a larger tip diameter. After a designated coagulation time, approximately 15 aggregates that had coagulated with YG beads were recovered and transferred into a clean 2% NaCl solution to prevent disaggregation. These aggregates were then individually collected and placed into another 2% NaCl solution

* Corresponding author voice: 520-621-4316; fax: 520-621-6048; e-mail: logan@engr.arizona.edu.

† Present address: Department of Civil and Structural Engineering, The University of Hong Kong, Pokfulam Rd., Hong Kong.

in a well plate (0.8 cm deep and 3.2 cm in diameter) to minimize aggregate disruption during subsequent microscopic examination. Aggregates that broke up during any transfer step were discarded.

Aggregate Characterization. The characterization of each recovered aggregate included the following: measuring its equivalent (cross-sectional area) diameter using an image analysis system (ScanArray II, Galai); counting the number of YG fluorescent beads captured by the aggregate under the fluorescent microscope using blue light; measuring the total solid volume of the red microspheres that formed the aggregate using a Coulter particle counter (Multisizer II, Coulter) after breaking up the aggregate as described in detail elsewhere (*13*).

Mean Shear Rates in the Jar-test Device. The experimental setup to measure the mean shear rate in the Jar-test device with a flat paddle was similar to that described by Lai et al. (16), except that a 1000-mL round beaker, filled with 500 mL of 2% NaCl solution, was used instead of a 2000-mL beaker. The mean shear rate of the fluid, G, at a paddle rotation speed, S (rpm), can be calculated (*16*) using

$$G = \sqrt{\frac{\pi S \Delta w g r_b}{30\,\mu V}} \tag{1}$$

where V is the liquid volume in the beaker, r_b is the beaker radius, Δw is the weight (measured by a balance) necessary to balance the torque produced by the paddle rotation, g is the gravitational constant (981 cm/s^2), and μ is the fluid viscosity. For our experimental conditions, $r_b = 5.38$ cm, $V = 500$ mL, and $\mu = 0.0095$ g/cm-s at 22.5 °C producing $G = 0.341(\Delta w S)^{1/2}$. Linear regression of log−log transformed data produced the correlation $\log G = -0.754 + 1.37 \log S$ ($n = 7$, $R^2 = 0.99$ for $3 \le S \le 30$). Stirring speeds were chosen to be large enough to keep particles suspended (a few rpm) but low in order to minimize aggregate breakup. The three stirring speeds of 6, 15, and 25 rpm used in this study are equivalent to mean shear rates of 2.1, 7.3, and 14.7 s^{-1}, respectively, resulting in a range of Reynolds numbers from 600 to 2400 where $Re = Sd^2_{pad}/v$, d_{pad} is the paddle diameter, and v is the kinematic viscosity. These average shear rates produce Kolmogorov microscales of 260−690 μm, which is in the range of the aggregate sizes examined.

Theoretical Section. *Collision Frequency Function for Permeable Fractal Aggregates.* For a binary system composed of two sizes of particles, large aggregates of diameter d_a and smaller particles of diameter d_p, the rate of the small particles captured by a single aggregate, R_c, can be written (*13*) as

$$R_c = \alpha(a,p)\beta(a,p)N_p \tag{2}$$

where a and p are subscripts referring to the aggregate and the smaller particles, β(a,p) is the collision frequency function between the aggregate and small particles, α(a,p) is the corresponding collision efficiency, and N_p is the concentration of the small particles. Several models can be used to calculate the collision frequency function. To distinguish between these models, a subscript is then added to β when it is predicted by the rectilinear (β_{rec}), curvilinear (β_{cur}), and fractal (β_{frac}) models, whereas β without a subscript indicates a measured collision frequency function.

According to the rectilinear model, collisions between large aggregates of size d_a and much smaller particles in an isotropic turbulent fluid occur with a frequency (*1*):

$$\beta_{rec} = \frac{1.3G}{8} d_a^{\,3} \tag{3}$$

This frequency differs from that predicted for laminar shear by the coefficient (1.3/8 versus 1/6 for laminar shear). While β_{rec} describes the average rate that fluid approaches an aggregate of diameter d_a (*1, 17*), the product $\beta_{rec}N_p$ is the number of small particles in the fluid approaching the aggregate per unit time.

The curvilinear collision model can be used to more accurately calculate the collision frequency function for impermeable spherical particles since this model takes fluid fields and short-range forces between approaching particles into account (*3, 5*). The collision frequency calculated using the curvilinear collision function, β_{cur}, is smaller than the rectilinear collision kernel by a factor e_{cur} or

$$\beta_{cur} = e_{cur}\beta_{rec} \tag{4}$$

Based on Han and Lawler's numerical solution for laminar shear (*5*)

$$e_{cur} = \frac{8}{(1+\lambda)^3} \exp[4.5 + 3.5 \log(\gamma) - \lambda(20.7 + 11.5 \log(\gamma))] \qquad (\text{for } \gamma < 0.01) \tag{5}$$

where $\lambda = d_p/d_a$, $\gamma = A/(18\pi\mu G d_a^2)$, and A is the Hamaker constant (assumed to be 4×10^{-20} J).

Highly porous fractal aggregates permit a significant quantity of fluid to flow through them, resulting in greater collision frequencies between the aggregates and small particles than predicted by the curvilinear collision model. β_{frac} can be related to β_{rec} using a fractal collision efficiency factor e_{frac} as

$$\beta_{frac} = e_{frac}\beta_{rec} \tag{6}$$

The fractal collision efficiency factor is a function of the fluid collection efficiency of the aggregate, e_f, defined as the ratio of the interior flow passing through the aggregate to the flow approaching it, e_p is the particle removal efficiency by the aggregate from the intra-aggregate flow, and α is the particle collision efficiency (*13*) according to

$$e_{frac} = \frac{e_f e_p}{\alpha} \tag{7}$$

The overall small particle capture efficiency of the aggregate, E, defined as the ratio of the particles captured by the aggregate to the total particles approaching it, is thus

$$E = e_f e_p \tag{8}$$

Calculation of Model Parameters from the Experiments. Assuming that the rate of small particles captured by an aggregate, R_c (eq 2), is constant over a short time period, T, the number of particles captured by the aggregate is $P_c = R_c T$ or $P_c = \alpha\beta N_p T$. Therefore, the collision frequency function between the aggregate and small particles can be calculated using

$$\beta = \frac{P_c}{\alpha T N_p} \tag{9}$$

In our experiments, T varied from 5 to 40 min, N_p varied from 10^5 to 5×10^5 mL^{-1}, and α was measured in a separate experiment as 0.237 (*13*).

During a time T while an aggregate is in a YG bead suspension, the total number of beads approaching the aggregate is $P_a = \beta_{rec}N_p T$. Thus, the overall small particle capture efficiency of the aggregate is $E = P_c/P_a$ or

$$E = \frac{8P_c}{1.3G d_a^{\,3} T N_p} \tag{10}$$

Results

Fractal Dimensions of Aggregates. From the slopes of the regression lines in Figure 1, the fractal dimensions of 435

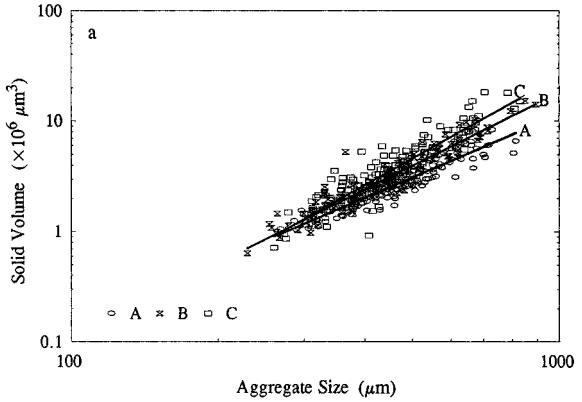

FIGURE 1. Average fractal dimensions of aggregates in groups of A, B, and C calculated from the slopes of the regression lines, $D_A = 1.89 \pm 0.06$ for group A aggregates, $D_B = 2.21 \pm 0.06$ for group B aggregates, and $D_C = 2.47 \pm 0.10$ for group C aggregates.

red-colored latex microsphere aggregates were 1.89 ± 0.06, 2.21 ± 0.06, and 2.47 ± 0.10 for the aggregates in groups A−C, respectively. The fractal dimension of aggregates in group A was significantly lower (slope comparison, $p < 10^{-4}$; *18*) than that in group B, and the fractal dimension of aggregates in group B was significantly lower (slope comparison, $p < 0.02$) than that in group C. Aggregates formed by relatively fast coagulation had the lowest fractal dimension, and aggregates formed by restructuring had the highest fractal dimension. The aggregate porosity increased with size and was inversely proportional to the fractal dimension with the porosities of all aggregates greater than 0.9 (*19*).

Collision Frequency Functions and Small Particle Capture Efficiencies of Fractal Aggregates. The number of YG beads captured by aggregates increased directly in proportion to the aggregate size and coagulation time, as shown in Figure 2a for one set of experiments (group A aggregates, $G = 2.1$ s^{-1}). As a result, data from different times were combined into a single data set in order to calculate the collision frequency functions between group A aggregates and YG beads at $G = 2.1$ s^{-1} using eq 9, as shown in Figure 2b. The same approach was used to calculate the collision functions for the other eight data sets of aggregate groups at the three different shear rates (Figure 3a−c). For aggregates having the same fractal dimension, higher shear rates produced higher collision frequencies between the aggregates and beads. The slopes of the collision functions versus aggregate size at different shear rates were not significantly different (slope comparison, $p > 0.32$), as seen from the nearly parallel regression lines in the same aggregate group (Figure 3), indicating a power law relationship between β and d_a.

In order to specify a correlation between β, G, and d_a, points taken from the regression lines (Figure 3) for three aggregate size classes (300, 500, and 700 μm) were plotted in terms of aggregate groups as a function of G (Figure 4). These size classes were chosen since the size range of 300−700 μm contained most of the aggregates (>90%) used in these experiments. The power law relationship, $\beta \sim G^m$, was demonstrated by the straight lines after a log−log transformation for the data of the three size classes (Figure 4). The powers, m, for the nine lines in Figure 4 were obtained from a linear regression analysis and plotted as a function of the fractal dimension (Figure 5). The regression of m versus D produced $m = (0.97 \pm 0.02) - (0.31 \pm 0.03)D$, indicating that m decreased in proportion to D. Due to the limited number of data for fractal dimensions, we chose $m = 1 - 0.33D$, resulting in

$$\beta \sim G^{1-0.33D} \tag{11}$$

Using this relationship, β in eq 11 is seen to be proportional

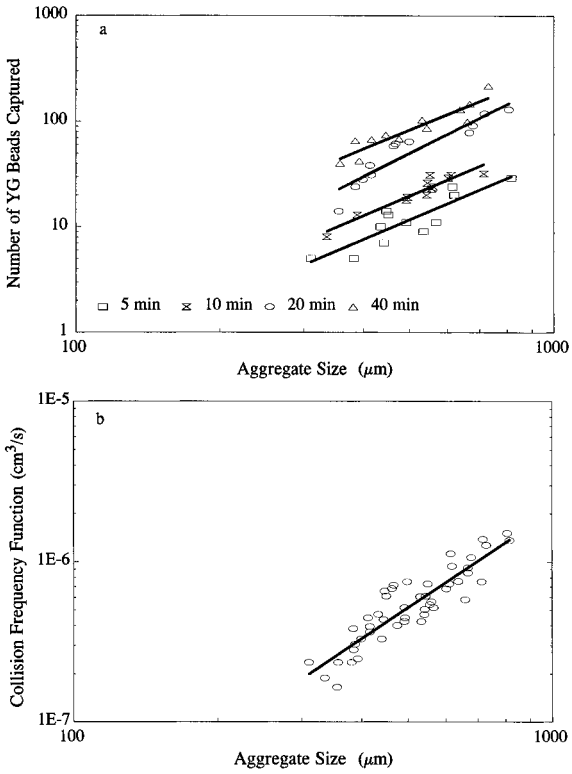

FIGURE 2. (a) Number of YG fluorescent beads captured by individual aggregates in group A at the shear rate of 2.1 s^{-1} as a function of aggregate size and coagulation time; (b) collision frequency function between group A aggregates and YG beads at the shear rate of 2.1 s^{-1}.

to G^1 for infinitely porous aggregates or when $D \rightarrow 0$, as described by the rectilinear model (eq 3). When aggregates are much denser and $D \rightarrow 3$, $\beta \sim G^0$ in eq 11, changes in the shear rate would not significantly alter collision frequencies as predicted by Han and Lawler (*5*) based on their curvilinear model calculations for impermeable particles.

Experimental results shown in Figure 3 support a power law relationship between the collision frequency function and both the aggregate size and fluid shear rate. We therefore assumed that $\beta = n_1 d_a^{n_2} G^m$, and from eq 11 $m = 1 - 0.33D$. To determine the empirical constants, n_1 and n_2, β was normalized for the mean shear rate using $\beta/(G^{1-0.33D}) = n_1 d_a^{n_2}$. The coefficients, n_1, and the powers, n_2, for the nine lines in Figure 3 were calculated using the regression analysis and plotted as a function of the fractal dimension (Figure 6a,b). Both terms decreased with D according to $\log(n_1) = -2.0 - 0.90D$ and $n_2 = 3.3 - 0.63D$, respectively, producing

$$\beta = 0.01 \times 10^{-0.9D} d_a^{3.3-0.63D} G^{1-0.33D} \tag{12}$$

with β (cm^3/s), d_a (cm), and G (s^{-1}).

A comparison of measured collision frequency functions (eq 12) with those predicted by the rectilinear and the curvilinear models indicates that β values were 5 orders of magnitude higher than β_{cur} but 2 orders of magnitude lower than β_{rec} (Figure 7). The overpredictions of the rectilinear model were expected since this model does not account for hydrodynamic interactions between approaching particles. In contrast, the curvilinear model underestimated β since it does not include a mechanism for flow through the aggregate. Recall that for this curvilinear model the collision frequency function does not increase in proportion to the mean shear rate.

Measured collision frequency functions less than β_{rec} indicated that not all small particles in the fluid approaching an aggregate were captured by the aggregate. The overall

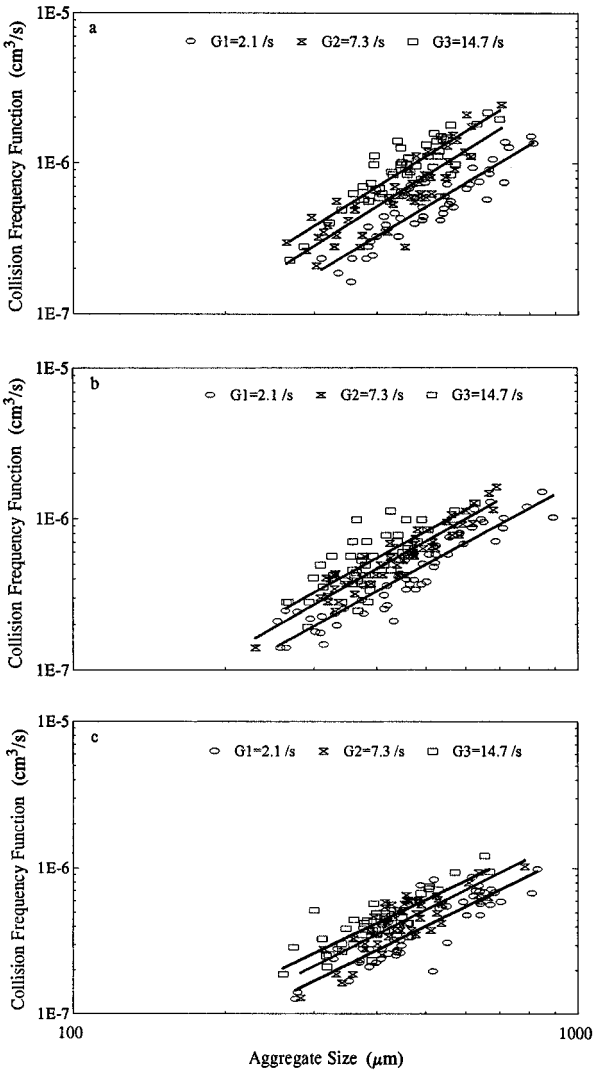

FIGURE 3. Collision frequency functions between YG beads and aggregates with fractal dimensions of (a) $D_A = 1.89 \pm 0.06$, (b) $D_B = 2.21 \pm 0.06$, and (c) $D_C = 2.47 \pm 0.10$. Solid lines were based on a linear regression for each data set at mean shear rates of 2.1, 7.3, and 14.7 s^{-1}.

small particle capture efficiencies, *E*, of the fractal aggregates used in this study were <1% and decreased with aggregate size (Figure 8). For a given size of an aggregate, E was inversely proportional to the fluid shear rate.

Discussion

Measured collision frequencies between large fractal aggregates and small particles in a turbulently sheared fluid were more than 5 orders of magnitude greater than those predicted by a curvilinear collision model that assumed the aggregates were impermeable spheres. We hypothesize that the differences between measured (β) and predicted (β_{cur}) collision frequency functions resulted from the significant permeabilities produced by the heterogeneous (fractal) distribution of primary particles within the aggregates. This hypothesis is based on similarly high collision frequencies (compared to curvilinear model predictions) observed for settling fractal aggregates having settling velocities faster than predicted by Stokes' law (*13*). Higher settling velocities were attributed to aggregate permeabilities greater than those predicted to occur when the primary particles of the aggregate were uniformly distributed throughout the aggregate. Our measurements in this study of β values much greater than β_{cur} under turbulent shear conditions were consistent with the high permeabilities of fractal aggregates (*13*).

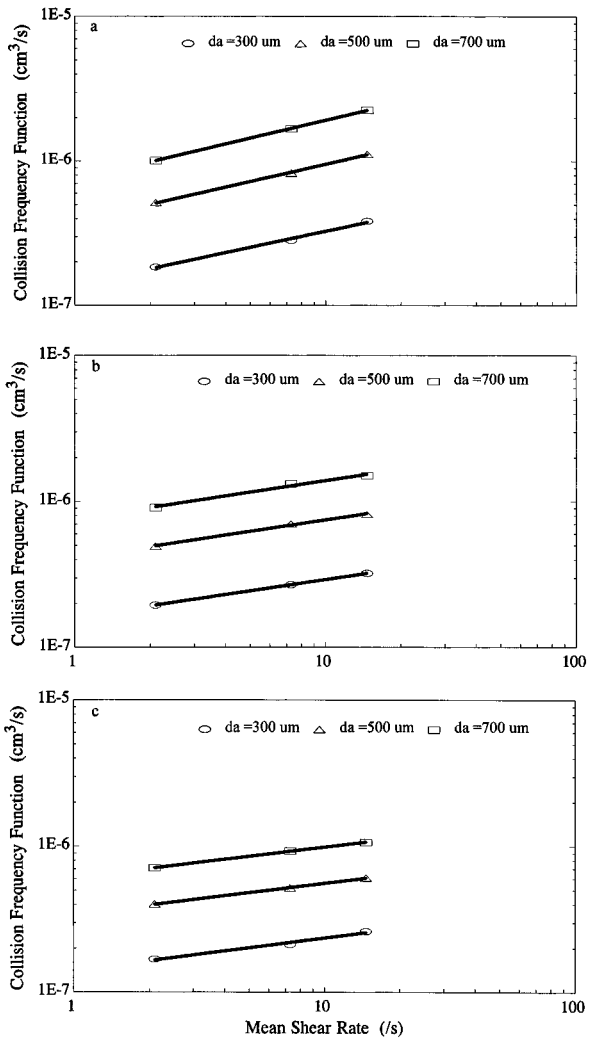

FIGURE 4. Relationship between the collision frequency function and the mean shear rate for the aggregates 300, 500, and 700 μm in diameter in (a) group A, (b) group B, and (c) group C.

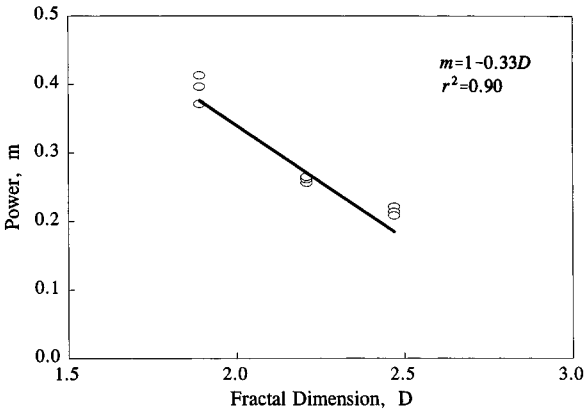

FIGURE 5. Power, *m*, in the power law relationship $\beta \sim G^m$ as a function of the fractal dimension.

Using a curvilinear collision model, Han and Lawler (*5*) argued that increasing the shear rate should not appreciably enhance flocculation in turbulent fluids. Their argument that β does not increase with G was developed for collisions between solid spheres. In the same manner as previous investigators (*3, 20*), Han and Lawler used a trajectory analysis to calculate β and assumed retarded van der Waals forces were the dominant attractive forces producing particle collisions. While high shear rates produce high relative velocities between approaching particles, the time available

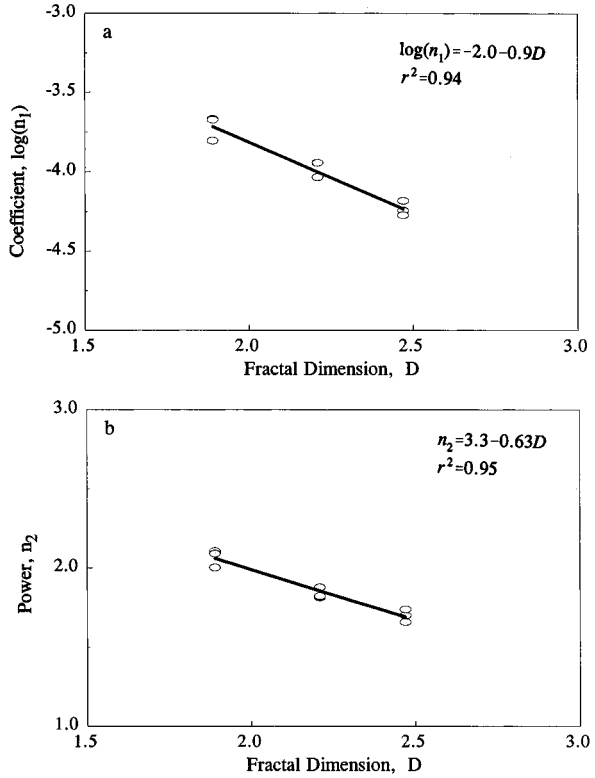

FIGURE 6. (a) Coefficient, n_1, and (b) the power, n_2, in the power law relationship $\beta/(G^{1-0.33D}) = n_1 d_a n^2$ as a function of the fractal dimension.

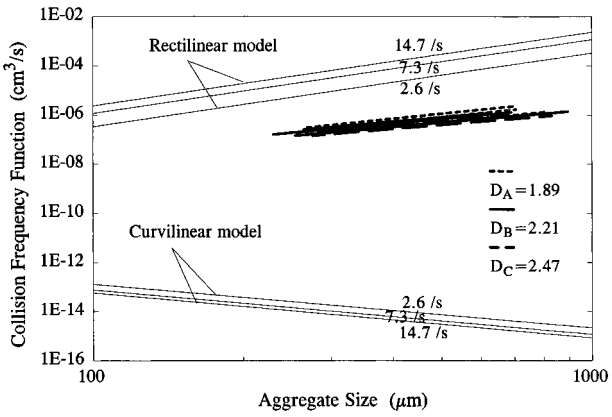

FIGURE 7. Collision frequency functions between fractal aggregates and YG beads in turbulent shear derived from experiments versus those predicted by the rectilinear and curvilinear models.

for these particles to overcome hydrodynamic effects at higher shear rates becomes shorter. Before the water separating the particles can be moved out of the way while van der Waals forces pull these particles together, the opportunity for collisions and adherence may have passed. Therefore, in contrast to the predicted increases in collisions by the rectilinear model, higher fluid shear rates would not promote any increases in particle collision frequencies between impermeable particles.

The different predictions of the rectilinear and curvilinear models on the importance of the shear rate can be partially resolved based on the magnitude of the particle fractal dimension. Han and Lawler's argument that the shear rate does not appreciably affect the coagulation rate was established for solid spherical particles, but it would also be consistent with our experimental results if aggregates had high ($D = 3$) fractal dimensions. For highly permeable fractal aggregates with lower fractal dimensions, however, the shear

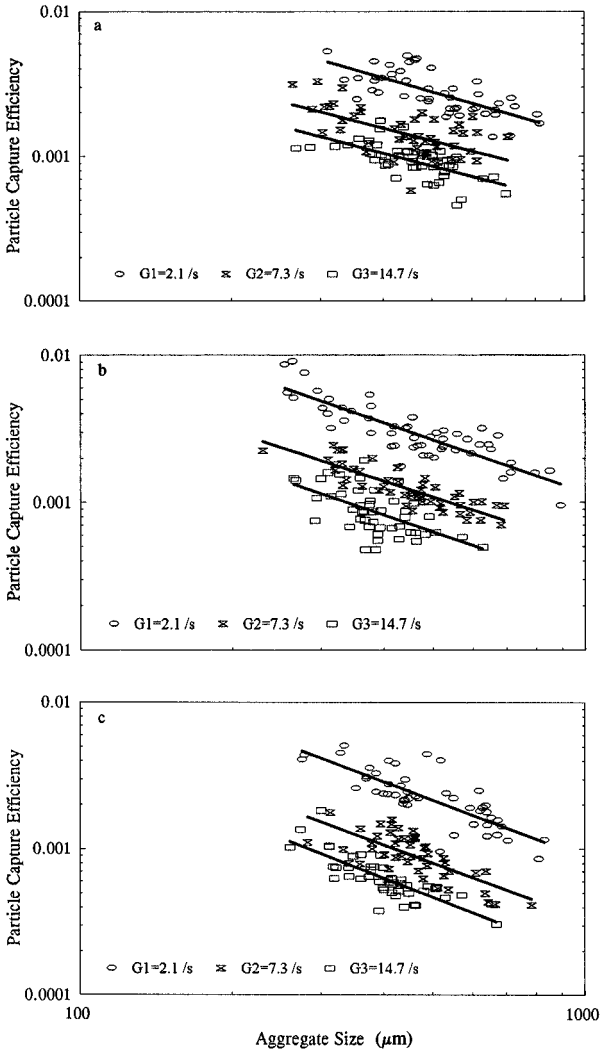

FIGURE 8. Overall bead capture efficiencies of the fractal aggregates in (a) group A, (b) group B, and (c) group C, respectively. Solid lines are regressions in terms of mean shear rates of 2.1, 7.3, and 14.7 s^{-1}.

rate will increase collision frequencies between the aggregates and small particles as shown by Figures 3 and 4.

The collision frequency function was found to be inversely proportional to the fractal dimension according to $\beta \sim G^{1-0.33D}$. At the limits of the range of fractal dimensions ($0 \leq D \leq 3$), β becomes a function of G in a manner consistent with either the rectilinear model or the curvilinear model. As $D \rightarrow 0$, aggregates become infinitely porous and the correlation between β and G approaches the rectilinear model prediction that $\beta \sim G$. It is a generally accepted theory regarding particle coagulation in water and wastewater treatment systems and in natural waters that G is an important parameter for enhancing coagulation (*2*, *21*, *22*). Our observations would support this theory only in systems dominated by coagulated and highly fractal particles. In instances where particle fractal dimensions are high and aggregates become denser and less permeable, β would be insensitive to the shear rate as predicted by the curvilinear model for the reasons discussed by Han and Lawler (*5*).

Although higher shear rates will increase collision functions (β) between fractal aggregates and other particles, particle capture efficiencies of these aggregates (E) will decrease with G (Figure 8). As previously discussed, any potential increases in particle collision frequencies caused by higher fluid velocities between approaching particles will be partially offset by less contact time between these particles. Thus, particle capture efficiencies of permeable aggregates decreased with the mean shear rates, as observed here in Figure 8.

The inverse effect of G on E can be mathematically demonstrated using a filtration model that describes particle removal by a porous medium. In a previous study, the fraction of mono-sized small particles in the interior flow captured by a settling fractal aggregate of size d_a was successfully described (*13*) using

$$e_p = 1 - \exp\left(-\frac{\zeta_1 \alpha \eta d_a}{d_c}\right) \quad (13)$$

where ζ_1 is a constant dependent only on aggregate properties such porosity, d_c is the size of the collectors within the aggregate, and η is the single collector efficiency. For suspended small particles, collisions are generated by diffusion and η can be described (*23*, *24*) by

$$\eta = 4\left(\frac{d_c U}{d_p}\right)^{-2/3} = \zeta_2 {d_c}^{-2/3} U^{-2/3} \quad (14)$$

where ζ_2 is a constant at a fixed temperature for a uniform suspension of monomers, and U is the average velocity of fluid flowing through the porous medium such as a porous aggregate. In a sheared fluid, U is related to the mean shear rate by $U = \zeta_3 G d_a$, where ζ_3 is a coefficient (*25*). Combining this with eqs 13 and 14 produces

$$e_p = 1 - \exp(-\alpha \zeta_1 \zeta_2 {\zeta_3}^{-2/3} G^{-2/3} {d_a}^{1/3} {d_c}^{-5/3}) \quad (15)$$

The size of principal collectors within a fractal aggregate can be written as $d_c = s{d_a}^b$, where s and b are empirical constants dependent on the fractal structure of the aggregate (*13*). Substituting eq 15 into eq 8 and letting $\zeta = -\alpha s^{-5/3} \zeta_1 \zeta_2 {\zeta_3}^{-2/3} {d_a}^{(1-5b)/3}$, we obtain the general expression for the particle capture efficiency of an aggregate of size d_a in terms of its fluid collection efficiency (e_f) and the mean shear rate as

$$E = e_f\left[1 - \exp\left(-\frac{\zeta}{G^{2/3}}\right)\right] \quad (16)$$

Thus, for a given aggregate, the particle capture efficiency decreases with the shear rate. Although the efficiency of particle capture decreases with the shear rate, an increase in G will still produce an overall increase in β, as previously shown by Figures 3 and 7 and by eq 12.

In summary, the high permeabilities and non-uniform distribution of primary particles in fractal aggregates resulted in increased collision frequencies between aggregates and small particles. The fluid shear rate played an important role in promoting coagulation between permeable aggregates and small particles, although the collision function was not linearly proportional to the mean shear rate as predicted by a rectilinear coagulation model.

Acknowledgments

This research was supported by ONR Grant N00014-91-J-1249.

Literature Cited

(1) Saffman, P. G.; Turner, J. S. *J. Fluid Mech.* **1956**, *1*, 16−30.
(2) Swift, D. L.; Friedlander, S. K. *J. Colloid Sci.* **1964**, *19*, 621−647.
(3) Adler, P. M. *J. Colloid Interface Sci.* **1981**, *83*, 106−115.
(4) O'Melia, C. R.; Tiller, C. L. *Environmental Particles, Vol. 2*; van Leeuwen, H. P., Buffle, J., Eds.; IUPAC Environmental Analytical and Physical Chemistry Series; Lewis Publishers: Chelsea, MI, 1993; pp 353−386.
(5) Han, M.; Lawler, D. F. *J. Am. Water Works Assoc.* **1992**, *84* (10), 79−91.
(6) Valioulis, I. A.; List, E. J. *Environ. Sci. Technol.* **1984**, *18*, 242−247.
(7) Hill, P. S.; Nowell, A. R. M. *Philos. Trans. R. Soc. London* **1990**, *A331*, 103−117.
(8) Veerapaneni, S.; Wiesner, M. R. *J. Colloid Interface Sci.* **1996**, *177*, 45−57.
(9) Li, D.; Ganczarczyk, J. J. *Environ. Sci. Technol.* **1989**, *23*, 1385−1389.
(10) Logan, B. E.; Kilps, J. R. *Water Res.* **1995**, *29*, 443−453.
(11) Li, X.; Logan, B. E. *Deep-Sea Res. Part II* **1995**, *42*, 125−138.
(12) Johnson, P. C.; Li, X.; Logan, B. E. *Environ. Sci. Technol.* **1995**, *30*, 1911−1918.
(13) Li, X.; Logan, B. E. *Environ. Sci. Technol.* **1997**, *31*, 1229−1236.
(14) Meakin, P. *Adv. Colloid Interface Sci.* **1988**, *28*, 249−331.
(15) Jiang, Q.; Logan, B. E. *J. Am. Water Works Assoc.* **1996**, *88* (2), 100−113.
(16) Lai, R. J.; Hudson, H. E., Jr.; Singley, J. E. *J. Am. Water Works Assoc.* **1975**, *67*, 553−557.
(17) Friedlander, S. K. *Smoke, Dust and Haze*; Wiley: New York, 1977; pp 187−189.
(18) Kleinbaum, D. G.; Kupper, L. L. *Applied Regression Analysis and Other Multivariable Methods*; Duxbury Press: North Scituate, MA, 1978; pp 95−102.
(19) Li, X. Ph.D. Thesis, University of Arizona, 1996.
(20) van de Ven, T. G. M.; Mason, S. G. *Colloid Polym. Sci.* **1977**, *255*, 468−482.
(21) Hudson, H. E., Jr. *J. Am. Water Works Assoc.* **1965**, *57* (7), 885−893.
(22) Hunt, J. R. *J. Fluid Mech.* **1982**, *122*, 169−185.
(23) Rajagopalan, R.; Tien, C. *Am. Inst. Chem. Eng. J.* **1976**, *22*, 523−533.
(24) Logan, B. E.; Jewett, D. G.; Arnold, R. G.; Bouwer, E. J.; O'Melia, C. R. *J. Environ. Eng.* **1995**, *121*, 869−873.
(25) Adler, P. M. *J. Colloid Interface Sci.* **1981**, *81*, 531−535.

Received for review September 9, 1996. Revised manuscript received December 12, 1996. Accepted December 16, 1996.[⊗]

ES960772O

[⊗] Abstract published in *Advance ACS Abstracts*, February 15, 1997.